Proceedings of GT2006
ASME Turbo Expo 2006: Power for Land, Sea and Air
May 8-11, 2006, Barcelona, Spain

GT2006-90752

INVESTIGATION OF 3D UNSTEADY FLOWS IN A TWO STAGE SHROUDED AXIAL TURBINE USING STEREOSCOPIC PIV AND FRAP

PART I: INTERSTAGE FLOW INTERACTIONS

L. Porreca[1], Y.I. Yun[2], A. I. Kalfas[1], S.J. Song[2], R.S. Abhari[1]

[1]*Turbomachinery Laboratory, Swiss Federal Institute of technology ETH Zürich*
[2]*School of Mechanical and Aerospace Engineering, Seoul National University, Seoul Korea*

ABSTRACT

A detailed flow analysis has been carried out in a two-stage shrouded axial turbine by means of intrusive and non-intrusive measurement techniques. Multi-sensor Fast Response Aerodynamic Probe (FRAP) and 3D-PIV system were applied at two locations downstream of the first and second rotors. Several radial planes were measured focusing on the blade tip region in order to obtain a unique set of steady and unsteady velocity data.

The investigation deals with the aerodynamics and kinematics of flow structures downstream of the first and second rotors and their interaction with the main flow in a partially shrouded turbine typical of industrial application. The first part of this work is focused on the flow field downstream of the first rotor while the second part studies the leakage flow in the cavity of the second rotor and its interaction with the main stream.

The interstage region is characterized by interactions between the tip passage vortex and a vortex caused by the recessed shroud platform design. Flow coming from the blade passage suddenly expands and migrates radially in the cavity region causing a localized total pressure drop. The time evolution of these vortical structures and the associated downstream unsteady loss generation are analyzed.

The partial shroud design adopted in this geometry is beneficial in terms of blade stress and thermal load; however flow field downstream of the first rotor is highly three dimensional due to the intense interaction between cavity and main streams. A flow interpretation is provided and suggestions for improved design are finally addressed based on the steady and unsteady flow analysis.

NOMENCLATURE

Cpt	Total pressure coefficient $(P_{0meas} - P_{SExit})/(P_{0Inlet} - P_{SExit})$
D	Trailing edge thickness
d	Diameter of the seeding particle in Eqs. 1,2
f	Frequency of the TE shed vorticity
I	Scattered light intensity
I_0	Maximum light intensity in Eqs. 1,2
Ma	Mach number
Pt	Total Pressure
Ps	Static Pressure
PS	Blade Pressure Side
Sr	Strouhal Number
SS	Blade Suction Side
u	Flow velocity
T/T_0	Blade passing period fraction
TE	Trailing Edge
x_0, y_0, z_0	Location of tracer particles in Eqs. 1,2
z	Turbine axial coordinate
Greek	
α	Angle between cameras A and B
Δz_0	Laser beam thickness
ε	Measurement Error
β	Pitch angle
ϕ	Yaw angle
Subscripts	
sec	Secondary flow vector
mean	Mean unit vector
Abbreviations	
FRAP	Fast Response Aerodynamic Probes
PIV	Particle Image Velocimetry
5HP	5 Hole Probe

INTRODUCTION

The flow within a multistage axial turbomachine is inherently unsteady and turbulent due to the interaction of wakes and secondary flow structures, shed by upstream blades, with the blades downstream. Furthermore, the incoming wakes are chopped by the rotor blades, and then diffuse and deform as they pass through the non-uniform pressure field in the blade passage. Those unsteady phenomena affect the performance of the airfoils and generate noise and structural vibration. Understanding of the unsteady flow physics is still a critical issue in rotating

turbomachinery and is thus a key requirement in achieving further improvements in performances.

Numerous experimental studies have already focused on flow interactions using miniaturized fast response aerodynamic probe devices (Schlienger et al. [1], Miller et al. [2]) to measure unsteady pressure as well as other flow field parameters. Recently, optical techniques like Particle Image Velocimetry (PIV) have also been applied to rotating machinery. However this measurement technique is still a challenge in such an environment because of the difficult optical access for the laser light and the need to use a particular calibration procedure to take into account the image distortion due to the cylindrical shape of the window. Moreover, since PIV measures the velocity field of traces added to the flow, achieving a uniform seeding with an optimum concentration is important. In large scale, rotating turbomachinery research facilities, these difficulties become even more critical. The main consequence of a non-uniform seeding is a spatial loss of data together with an increased level of uncertainty in the measurement field.

For those reasons, very little has been published on successful application of PIV to turbomachinery. Wernet [3], Balzani et al. [4], Sanders et al. [5] and Uzol et al. [6] focused on the 2D flow field in axial and centrifugal compressors, studying both steady state and transient flows. Göttlich et al. [7] and Liu et al. [8] performed stereoscopic PIV measurements focusing on the wake-wake interaction at midspan in an axial transonic turbine and in the tip region of an axial compressor respectively.

In this work, an extensive application of Fast Response Aerodynamic Probe (FRAP) and Stereoscopic PIV has been carried out in a two-stage shrouded axial turbine. The investigation is focused on the flow in the interstage region and in the downstream region. A unique measurement data set has been acquired using stereo PIV in the tip leakage path at the exit of the turbine.

Part I of the paper deals with aerodynamics and passage flow structures in the interstage region. The flow evolution in the cavity region is described in detail in Part II of this paper. The adopted partial shroud ensures a lower level of mechanical stress in the blade root. However, the resultant flow field is highly three dimensional. The coupling between flow kinematics and loss generation is therefore investigated to gain deeper understanding of flow physics and to suggest ways to improve aerodynamic design of blade/shroud components.

EXPERIMENTAL METHOD

The research facility

The experimental investigation has been performed on the research turbine "LISA" at the Turbomachinery Laboratory of the ETH Zurich. The facility can accommodate a maximum of two stages of an axial turbine. The air-loop is of a closed type and includes a radial compressor, a two-stage water to air heat exchanger and a calibrated venturi nozzle for accurate mass flow measurements. A DC generator absorbs the turbine power and controls the rotational speed of the turbine shaft. The first and second rotors are mechanically decoupled by a twin spool shaft design. A pair of independent torquemeters allows to derive separately the torque of each. To achieve the same rotational speed, both shafts are coupled again before the DC generator. A sketch of the turbine section is presented in Fig 1. More details can be found in Porreca et al. [9].

The turbine design allows quick and precise assembly and an easy access to the measurement planes. A number of different intrusive (probes) and non-intrusive measurement (PIV) techniques are applied. The facility is equipped with a 4-axis numerically controlled positioning system with ultra high precision in every direction. The turbine is normally operated at constant pressure difference across the stages. The turbine entry temperature is controlled to an accuracy of 0.3% and the RPM is kept constant by the DC generator with a range of ±0.02% (± 0.5 RPM). The main operational parameters of the facility are listed in Table 1. The test case under investigation is representative of a partially shrouded axial turbine for power generation and is sketched in Figure 1.

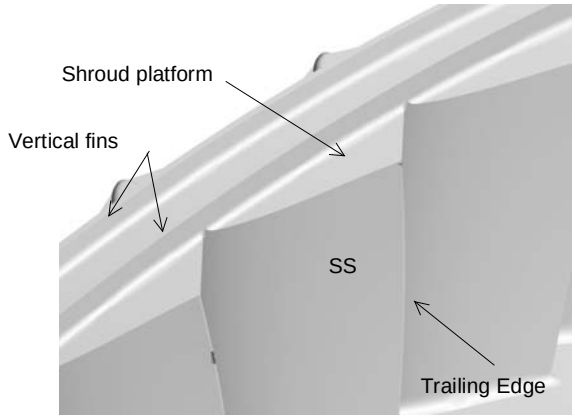

Fig. 1 Schematic of the rotor partial shroud geometry

The partial shroud has two vertical fins and a shroud platform with cutbacks at leading and trailing edges. The tip clearance in both rotors is 1% of the blade span.

Rotor speed [RPM]	2625
Overall pressure ratio	1.38
Mass flow [kg/s]	10.65
Blade count (Stator/Rotor)	42 / 42
Aspect ratio	1.8
Outer tip diameter [m]	0.8
Mach number (Stator/Rotor)	0.35 / 0.1
Reynolds number (Rotor)	$2*10^5$

Table 1: Main parameter of "LISA" 2-stages Axial turbine research facility.

Measurement technology

Stereoscopic PIV: The 2-stage axial research turbine rig "LISA" has been equipped with a 3D-PIV optical measurement system. Stereoscopic PIV technology has been applied to compensate for perspective error (Prasad [10]) as well as to observe highly three-dimensional flows in turbomachinery. Two optical windows made of acrylic PMMA are installed in the test turbine as shown in Fig. 2.

The window surface has been carefully polished to achieve good transparency. The windows are located between the first rotor and the second stator as well as downstream of the second rotor. The windows are designed to reproduce the exact shape of the double curvature contoured casing inner wall.

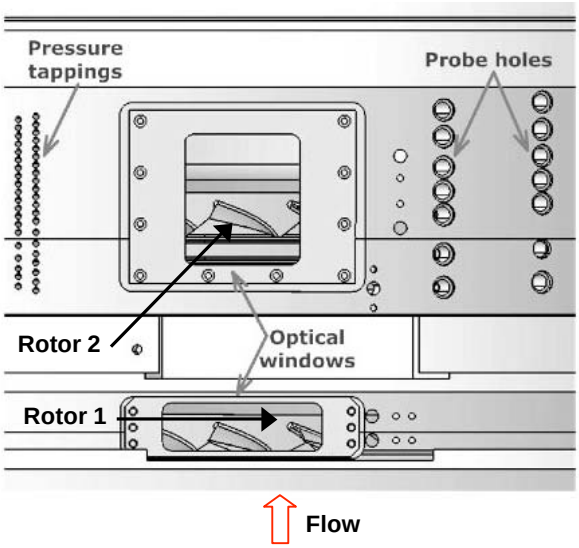

Fig. 2: Optical windows and probe holes in the test turbine

The flow was seeded with fine oil DEHS particles generated by a Laskin nozzle (Kähler et al. [11]). To obtain a uniform concentration an injection device was designed to seed the entire air mass flow.

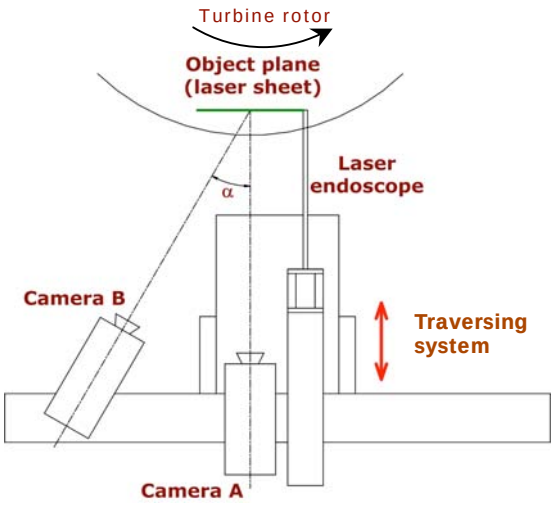

Fig. 3: Stereoscopic camera configuration in the test turbine

Deposits of seeding material on the casing windows were not significant during the operation. The nominal particle diameter was around 1 μm which is considered as adequate (according to Mellin [12]) for a frequency response up to 10 kHz.

The digital images are recorded with 1280x1024-pixel 12-bit CCD cameras (PCO SensiCam SVGA) whose pixel size and pitch are 6.7x6.7 μm and 9 μm, respectively. The cameras are set taking into account the Scheimpflug condition (Zang and Prasad [13]). Nikon AF MICRO NIKKOR lenses with a focal length of 60 mm are used for camera optics. A double-cavity Nd:YAG laser (Solo120PIV, New Wave Research) is used as a light source. The laser generates a maximum of 120 mJ/pulse of 532 nm wavelength green visible light. The pulse width is 10 ns, and the repetition rate is 15 Hz. The bursts of laser light are synchronized with cameras via a Dantec FlowMap system hub. The laser beam is delivered to a laser endoscope (ILA Intelligent Laser Applications) through an articulated mirror arm. The laser endoscope not only generates laser sheet through a cylindrical lens but also bends the laser sheet by 90° with a prism at the tip. The outer diameter of the laser endoscope is 8 mm and the divergence angle of the laser sheet is approximately 16°. The cameras and laser endoscope are mounted on a motor-controlled 1-axis linear stage so that cameras and the light sheet move together in the radial direction (Fig. 3).

By traversing radially the entire system, several blade-to-blade planes can be illuminated with a laser endoscope. Camera A is positioned such that its axis is perpendicular to the light sheet plane to avoid an interference with the laser endoscope. Camera B is tilted by different angles (22°, 25°, 30°) as shown in Fig. 3. The image plane (CCD plane) of camera B is further rotated by 5° to satisfy the Scheimpflug condition which ensures that all particles in the object field will be in good focus in the image plane (Prasad [10]). To compensate for the perspective distortion of the field of view due to the tilted angle of camera B as well as optical distortion through the double-curvature windows, a three-dimensional calibration method is used.

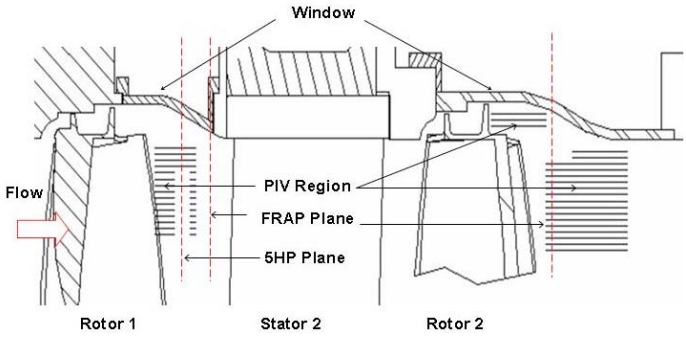

Fig. 4: Measurement regions: PIV, FRAP and 5HP planes

However in the interstage area, the region of the window with abrupt change of curvature provides a severe optical distortion that could not be corrected by the calibration procedure. Therefore, data measured in this region have been blanked. The details on the calibration method can be found in Soloff et al. [14].

Figure 4 shows the measurement planes of FRAP and 5HP probe and the PIV region at the interstage and at the turbine exit region. The first stator is not shown in the figure for a better visualization of the measurement areas. Regarding the interstage region, measurements were taken in 15 blade-to-blade planes from 66 to 97 percent span. One blade passing period is divided into 20 time steps, and between 60 and 100 digital image pairs for each

measurement plane at each time step are recorded of a 50x40 mm^2 area in the flow. For the downstream region, measurements are done on 3 planes inside the shroud cavity and 17 blade-to-blade planes (from 60 to 96 percent span) downstream of the second rotor. One blade passing period is divided into 10 time steps, and 100 image pairs are recorded on each plane at each time step.

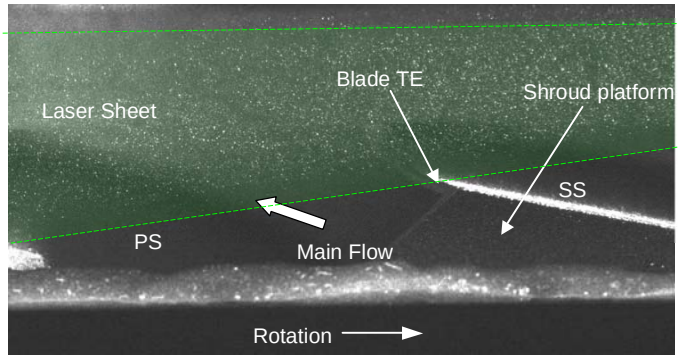

Fig. 5: Recorded image of seeded flow in the interstage measurement region

The time interval between two bursts varies between 2 and 4 μs depending on the average flow field velocity. Each pair of images is interrogated using cross-correlation analysis in 32x32-pixel sub-images with an overlap of 50 percent between adjacent interrogations. An advanced interrogation method of window offset (Westerweel et al. [15], Scarano and Riethmuller [16]) is used. The theoretical analysis and simulations performed by Westerweel et al. [15] show that the signal-to-noise ratio with window offset is approximately three times larger than that without window offset for flow with high turbulence intensity. Furthermore, the method of window offset is effective to reduce the error due to *loss-of-pairs*. To filter out spurious data, the local median is used (Westerweel [17]). Figure 5 shows a recorded image in the interstage measurement region. Visible in the picture are the blade trailing edge, the shroud platform, and the seeding illuminated by the laser beam.

Uncertainty analysis of PIV Measurements: For the estimation of the uncertainty of PIV velocity measurements many parameters have to be considered (Raffel et al. [18] Willert and Gharib [19]):

- Particle image diameter
- Displacement of the particle relative to the interrogation area size
- Particle image density
- Local velocity gradients
- Out-of-plane motion of tracer particles
- Background noise

There is no established method to analytically evaluate the uncertainty of PIV due to the above factors. Therefore, the assessment of PIV accuracy should be done for each PIV system by using one of the following three methods. The first method is to measure a flow field with an exact solution (e.g. Poiseuille flow or three-dimensional rotating disk flow) with PIV and to evaluate uncertainty for the flow field. However, it is difficult to guarantee whether the evaluated uncertainty for a specific flow field can be applied to other flow fields. Also, it is not always possible to introduce those flow conditions with exact solutions in a specific environment such as the current test rig. The second method is to conduct a Monte Carlo simulation of particle displacements (Keane and Adrian [20], Raffel et al. [18]). By conducting this simulation, more diverse flow fields can be tested. Third, PIV results can be compared against data obtained with hot wire or pneumatic probe technology or direct numerical simulation (Scarano and Riethmuller, [16]). However, rigorous evaluation of uncertainty is difficult with this method.

In the current investigation, a Monte Carlo simulation has been conducted to evaluate measurement errors of PIV. To carry out a Monte Carlo simulation, tracer particle images must be artificially generated. The light intensity scattered from individual tracer particles is assumed to have a Gaussian profile as

$$I(x,y) = I_0 \exp\left[\frac{-(x-x_0)^2 - (y-y_0)^2}{(1/8)d^2}\right] \qquad (1)$$

The laser light is also assumed to have a Gaussian profile in the out-of-plane direction.

$$I(z) = I_0 \exp\left[-\frac{z_0^2}{(1/8)\Delta z_0^2}\right] \qquad (2)$$

The location of each tracer particle (x_0, y_0, z_0) is set by using a random number generator. Then, the light intensity scattered from the particle at each location in an interrogation area can be defined from Eqs. (1) and (2). Four parameters—particle image diameter, number of particles, maximum light intensity I_0 and actual displacement— must be given a priori. The diameter of tracer particles has been set such that it occupies a 2×2 pixel or 3×3 pixel region. The number of particles has been set at 50. Both parameters have been determined via a trial-and-error process so that the artificially generated particle images look similar to the images actually taken during the measurement. Based on these, the first and second image frames with a time interval between 2 and 4 μs can be generated. The actual displacement of the particle ($\Delta x, \Delta y, \Delta z$) is taken from a representative averaged velocity value measured with PIV at each point of interest. Based on this displacement value, the image pairs of tracer particles in the object plane can be generated.

The particle images have not been generated in the entire field of view (for the current investigation, 50×40 mm) but at three points. One point in the field of view corresponds to a 32×32 pixel interrogation window in the image plane. However, the particle images have been generated in a 96×96 pixel region to properly take account of particles entering and exiting the 32×32 pixel interrogation area located at the center of the 96×96 pixel region. With stereoscopic PIV, the displacement values seen by two cameras are different, particularly when there are out-of-plane displacement components. Also, perspective and optical distortions of the images occur when the particle images are projected onto the image planes. The calibration procedures have been used to

estimate not only the image distortions but also displacement values seen by both cameras' image planes. The interrogation area is also subject to background noise due to reflection on solid surfaces and the light scattered from tracer particles located outside the light sheet. Therefore, the background noise has a certain static intensity level (from the reflection) as well as a randomly moving pattern (from the scattering of particles outside the light sheet). To obtain a spatially random intensity pattern, a random number generator has been used. Then, the background noise is superimposed on the particle images. Because there is a randomly moving pattern in the background, the noise patterns for the first and the second frames have been separately generated. 300 particle image pairs for each point have been generated to carry out statistical evaluations. The stereoscopic PIV error has been evaluated comparing the actual displacement imposed and the resultant values calculated using the artificially generated images. The measurement error consists of *bias error* and *root-mean-square* (*rms*) *error* (Raffel et al. [18]).

$$\varepsilon_{PIV} = \varepsilon_{bias} + \varepsilon_{rms}$$

Bias error is defined as the difference between the actual velocity value and the averaged value measured with PIV. Bias error originates from loss-of-pair and velocity gradients in interrogation areas.

Interstage Region

		Velocity [m/s]			
Span		*Tang. Velocity*	*Axial Velocity*	*Radial Velocity*	*Yaw Angle [°]*
96%	Actual values	**30**	**-5**	**10**	**80.54**
	Mean	28.31	-3.91	8.31	82.16
	St deviation	3.09 %	-14.23 %	24.72 %	1.62 %
	Bias Error [m/s]	**1.7**	**-1.09**	**1.7**	**-1.63**
66%	Actual values	**30**	**65**	**10**	**24.7**
	Mean	28.32	62.99	16.59	24.22
	St deviation	7.53 %	4.15 %	50.97 %	7.80 %
	Bias Error [m/s]	**1.68**	**2.01**	**-6.59**	**0.55**

Turbine exit region

		Velocity [m/s]			
Span		*Tang. Velocity*	*Axial Velocity*	*Radial Velocity*	*Yaw Angle [°]*
85%	Actual values	10	30	5	18.43
	Mean	13.09	31.10	1.08	22.83
	St deviation	19.9 %	11.6 %	11.88	18.0 %
	Bias Error [m/s]	**3.09**	**1.10**	**-3.92**	**4.40**

Table 2: Uncertainty Analysis for Stereoscopic PIV measurements

Rms error is the standard deviation of the values measured with PIV and can be regarded as measurement uncertainty of PIV. Table 2 shows the resulted values from the uncertainty analysis expressed in bias and rms error performed in the interstage and turbine exit region. Results for the cavity region are presented in Part II of the present work [25].

The bias error at the interstage region for the axial and tangential velocity (in plane component with respect to the laser light sheet) is always in the range of +/- 2 m/s. Standard deviation is in the range of 4 - 7% at the lower span and higher close to the tip where absolute velocity magnitude is smaller. In the turbine exit region, similar values are obtained with a higher values of the rms.

The bias error of the radial velocity (out-of-plane component) is more than 10% in all the planes, therefore, the radial velocity ought to be assessed only qualitatively. Another trend is that the errors of the in-plane components (tangential and axial velocities) are similar for all three locations while the error of the out-of-plane component increases as the measurement location becomes farther from the optical window. Measurement planes farther from the window suffer from severer optical distortion. Thus, the error of the out-of-plane component appears to be more susceptible to optical distortion. Lower error on the out-of-plane component could have been achieved by increasing the angle between the cameras (Lawson and Wu [21]). However this solution resulted to be not feasible in the current set up due to the laser endoscope (Figure 5).

FRAP 2-Sensor and pneumatic probe: Flow parameters including total and static pressure, flow angles, velocity components, and Mach numbers are measured at frequencies of up to 40 kHz using a 2-Sensor Fast Response Aerodynamic Probe (2S-FRAP). This probe is a modified version of the conventional single sensor probe with a second sensor sensitive to pitch angle variations of the flow and has been used in previous investigations (Porreca et al. [22]). The FRAP probe technology also provides unsteady temperature measurements at a low frequency of up to 10Hz. The absolute uncertainties are listed in Table (4?). Temperature measurements obtained with FRAP are affected by an absolute uncertainty of the order of ±0.3 K.

The measurement grid comprises 1502 points distributed uniformly in the circumferential direction every 3.5% pitch (32 point in 1.1 pitches) and 47 points in the radial direction, clustered towards the endwalls. Data from the probe sensors are sampled at 200 kHz corresponding to 109 samples for each blade passing period. Phase-locked averaging data procedure is done over 80 rotor revolutions.

Steady state measurements are performed using miniaturized pneumatic 5-Hole-Probes with a 0.9 diameter cobra head shape (Treiber et al. [23]). The probe is calibrated with a range of +/- 14° yaw angle and +/- 30° pitch angle. Uncertainty of pneumatic probes is reported in Table 3 in a calibration range of +/- 10° yaw angle and +/- 10° pitch angle. For higher pitch angle, higher uncertainty is detected.

Probe Type	ϕ	β	*Pt*	*Ps*	*Ma*
5HP	0.3°	0.3°	60 Pa	130 Pa	0.4%
FRAP-2S	0.3°	0.3°	100 Pa	150 Pa	0.5%

Table 3: Uncertainty bandwidth of pneumatic 5HP and 2S-FRAP

FRAP – 3D PIV COMPARISON AND ANALYSIS

Figure 6a,b shows a comparison between the velocity measured by the 3D PIV technique (a) and the FRAP data (b). FRAP data are presented in the same domain than the PIV measured region. Regions with insufficient laser illumination are blanked at the left and right borders. Both pictures are presented with the same scale and levels. The

higher tangential velocity region on the middle of the pictures shows the presence of the tip passage vortex occurring between 0.8 and 0.9 span height. The comparison shows a good agreement between the two measurement techniques. In the PIV plot, the high tangential velocity core is slightly larger with respect to the FRAP measurements, however location of the vortex and absolute the core middle, differences are limited in the range of +/- 1.5 m/s that is in agreement with the uncertainty detected in the PIV measurements shown in the previous section.

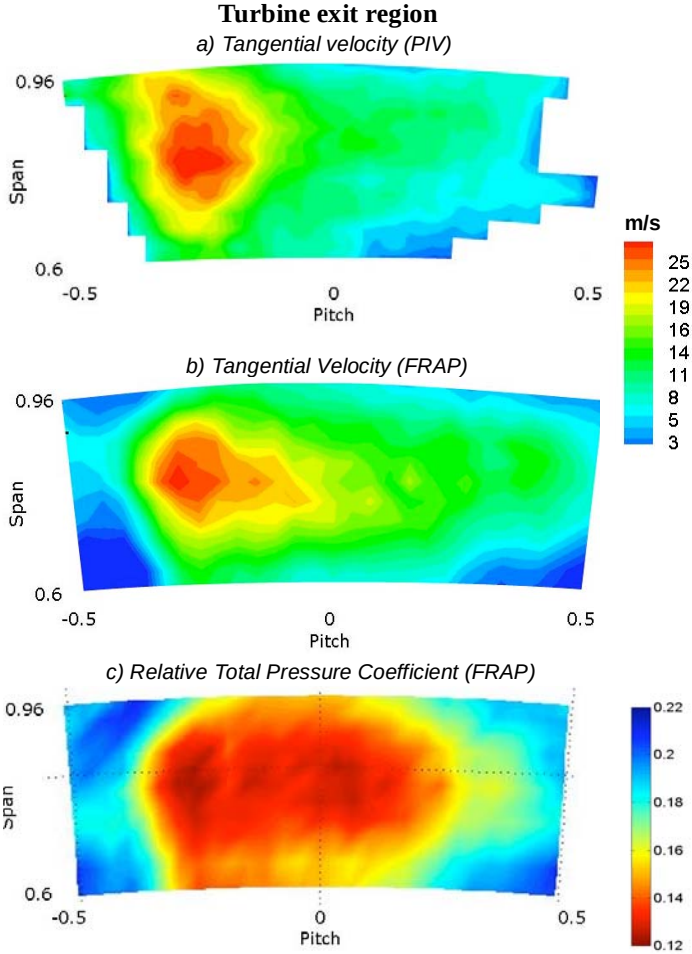

Fig. 6: Measured absolute tangential Velocity a) PIV b) FRAP c) FRAP Relative Total Pressure Coefficient at one rotor blade position – Turbine exit region

Figure 6c shows the relative total pressure coefficient measured by the FRAP probe at the same blade position. Corresponding with the underturning flow region, a local relative total pressure reduction is measured. Figure 7a shows the pitchwise yaw angle on different axial planes downstream the second rotor blade. The time averaged FRAP and PIV data are presented together with 5-Hole-Probe measurements. Because of blanked regions on the PIV set at the FRAP and 5HP measurement plane (153% tip axial chord) the data are presented on planes farther downstream starting form 171% to 208% distance. A good agreement again is observed between the probe and the optical measurement techniques. Underturning – overturning behavior is observed from 0.7 span up to the blade tip where the design intention is to align the flow with the underturned leakage flow in order to minimize mixing losses. Yaw angle profile measured by the probes (FRAP and 5HP) lays on the same line up to 0.75 span, then small discrepancies of about +/- 1.5° are observed up to the blade tip. Due to the high unsteadiness generated by the passage vortex in this region the time averaged signal of a fast response probe does not necessarily coincide with the pneumatic average of the 5HP.

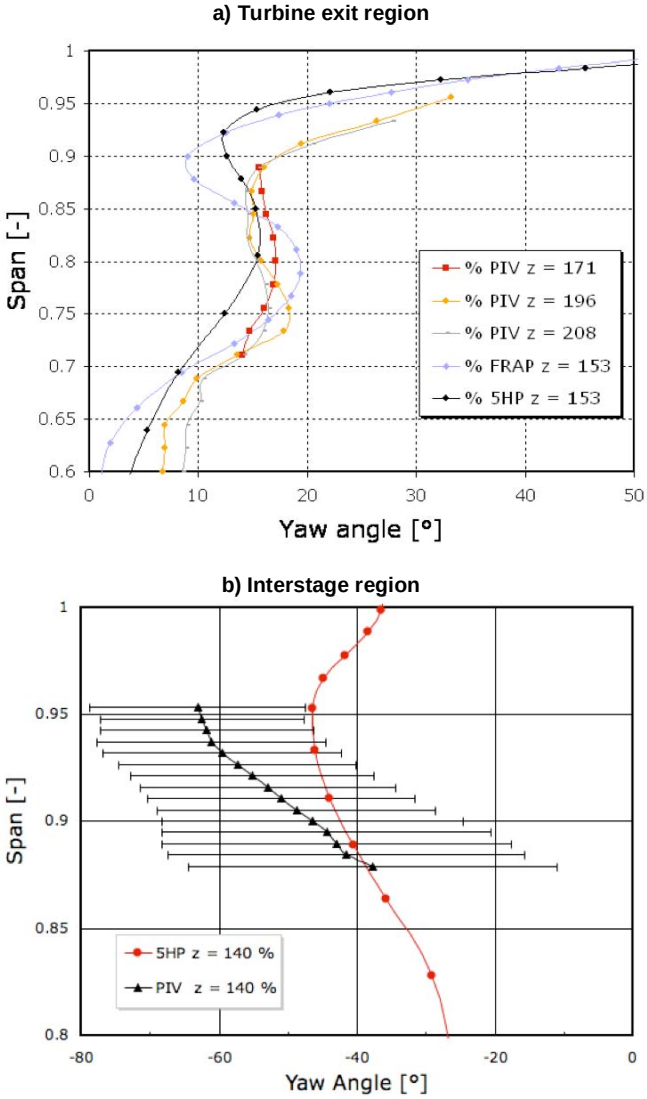

Fig. 7: Comparison between FRAP and PIV measured time averaged pitchwise yaw angle a) Turbine exit region b) Interstage region – black bars represent range of variation

The PIV time averaged data are in good agreement with the probe data. Differences are of the order of +/- 2.5° in the region up to 0.9 blade span. Above 90% span, in the area of overturning due to the leakage layer, the trend is captured correctly but higher differences with probe data are detected. The PIV data have a shift in the lower section of the blade span. This behavior may be explained by taking into account that farther downstream of the blade row (up to z=208% tip axial chord) the leakage layer is more entrained in the main flow. It is interesting to note that FRAP and 5HP results are consistent throughout but the PIV results vary in comparison. The greatest variation is in the vicinity of the passage vortex

core, where perhaps the errors in the out-of-plane velocity component in the PIV data contribute to the observed variation.

Figure 7b shows a comparison between the 5HP data and time averaged PIV data downstream the first rotor at the same axial location (140% tip axial chord). Due to the second stator row and the significant interaction between the main flow and leakage flow, this region is affected by a high degree of unsteadiness. Moreover, due to the countered enwall, very high pitch angle has been measured close to the tip with an averaged value of -30° at the limit of the 5HP calibration map. Flow features in this region, are entrained into the main flow as shown later on (Figure 11).

Horizontal bars on the PIV data points represent the range of variation of the measured yaw angle during one blade passing period. Higher differences are observed in the comparison between 5HP and time averaged PIV data with respect to the turbine exit region. Specifically, the pneumatic averaged data from the 5HP appear to move towards the lower yaw angle values. However, at every span location, the 5HP data lay within the range of variation of the PIV data. Unsteady FRAP data are not available from this axial plane.

INTERSTAGE FLOW ANALYSIS

Figure 8 shows the pitchwise time averaged yaw angle in different axial planes downstream of the first rotor blade from 127% to 150% tip axial chord. In all planes a large flow underturning and overturning occurs from 70% span to the tip due to the passage vortex. In the downstream axial planes from 127% to 150% an increasing region of underturning is visible in the tip region due to the incoming tip leakage layer flow. In the labyrinth seal, the flow still has a high momentum in the tangential direction given by the upstream NGV's. Therefore at the exit of the rotor blades, the main stream and the leakage have a high difference in tangential momentum that results in an increase in mixing losses. For this reason some designs adopt "bladelets" to turn the leakage flow and reduce the gradient in tangential velocity (Wallis et al., [24]). However, no clear improvement has been reported due to the poor performances of the turning devices installed in the shroud.

Figure 9 shows the measured absolute yaw angle and the projection of the velocity vectors in a radial plane at different blade span positions from 73% to 96 % span. The yellow region in the middle of the data set is blanked because of severe optical distortion due to the optical window as already mentioned. All pictures are taken at one blade rotor phase locked position and are the results of averaging 100 samples. At 77% span the yaw angle distribution shows clearly two main regions: the main "undisturbed" flow in the middle of the passage and the wake region. In the region close to the trailing edge the axial velocity deficit in the wake is creating a large area of underturned flow up to +80° with a high angle gradient in the circumferential direction. The underturning behavior is also in the tip passage vortex that occurs in this area.

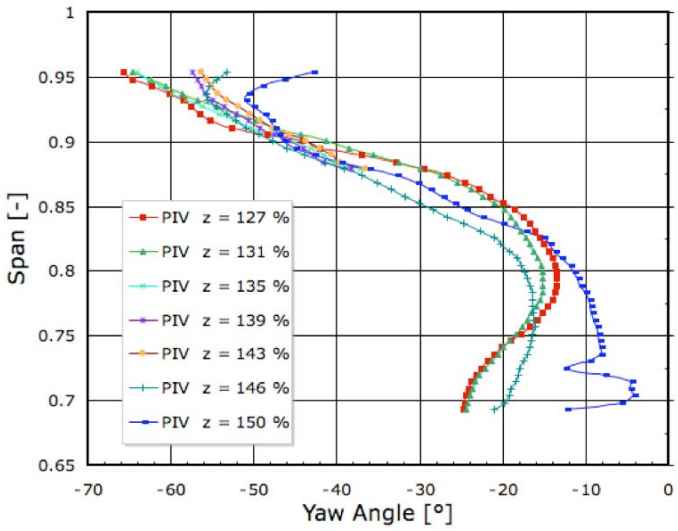

Fig. 8: PIV measured time and pitchwise averaged absolute yaw angle at different axial plane – Interstage region

Moving radially outward towards the blade tip, the area of underturned flow is gradually reduced until 91% span where a small influence of the wake is still present. At higher blade span locations a strong overturning occurs due to the passage vortex. Moreover at 96% span near the suction side a small negative axial velocity component is measured (Figure 9 and 10). The sudden expansion of the flow in the blade passage due to the uncovering of the shroud platform on the suction side is responsible for this behavior. The passage vortex after the blade throat grows, and expands over the shroud platform. A radial upward motion together with a backward axial migration of the main flow in the cavity region is detected as shown in Fig 9 and 10 where yaw angle larger then 90° is measured in the upper span region. This motion occurs mainly downstream the trailing edge and is weaker in the middle of the passage. Similar behavior is observed also in the measurements performed in the leakage cavity downstream of the second rotor where the shroud has similar geometry. A detailed description of this process is reported in Part II of this paper [25].

Figure 10 shows measured yaw angles in axial planes cuts at one rotor position from 122% to 129% tip axial chord distance. A dashed line shows the downstream projection of the blade trailing edge. The rotor is moving from the right to the left. Only one half of the blade pitch is represented to focus the attention on the wake – secondary flow region. A large flow angle gradient is observed between 80% span and the tip of the blade where the yaw angle varies from –80° to 40°. This gradient is higher at 119% tip axial chord position (closer to the blade) and continuously decreases moving downstream due to the mixing process. This large gradient in yaw angle is created by the tip passage vortex that occurs at this location. In the blade trailing edge region a radial migration of the flow is observed towards the tip due to a deficit of tangential momentum. A marked radial velocity gradient is observed moving from the main flow to the wake region that generates shed streamwise vorticity with an opposite sign with respect to the passage vortex.

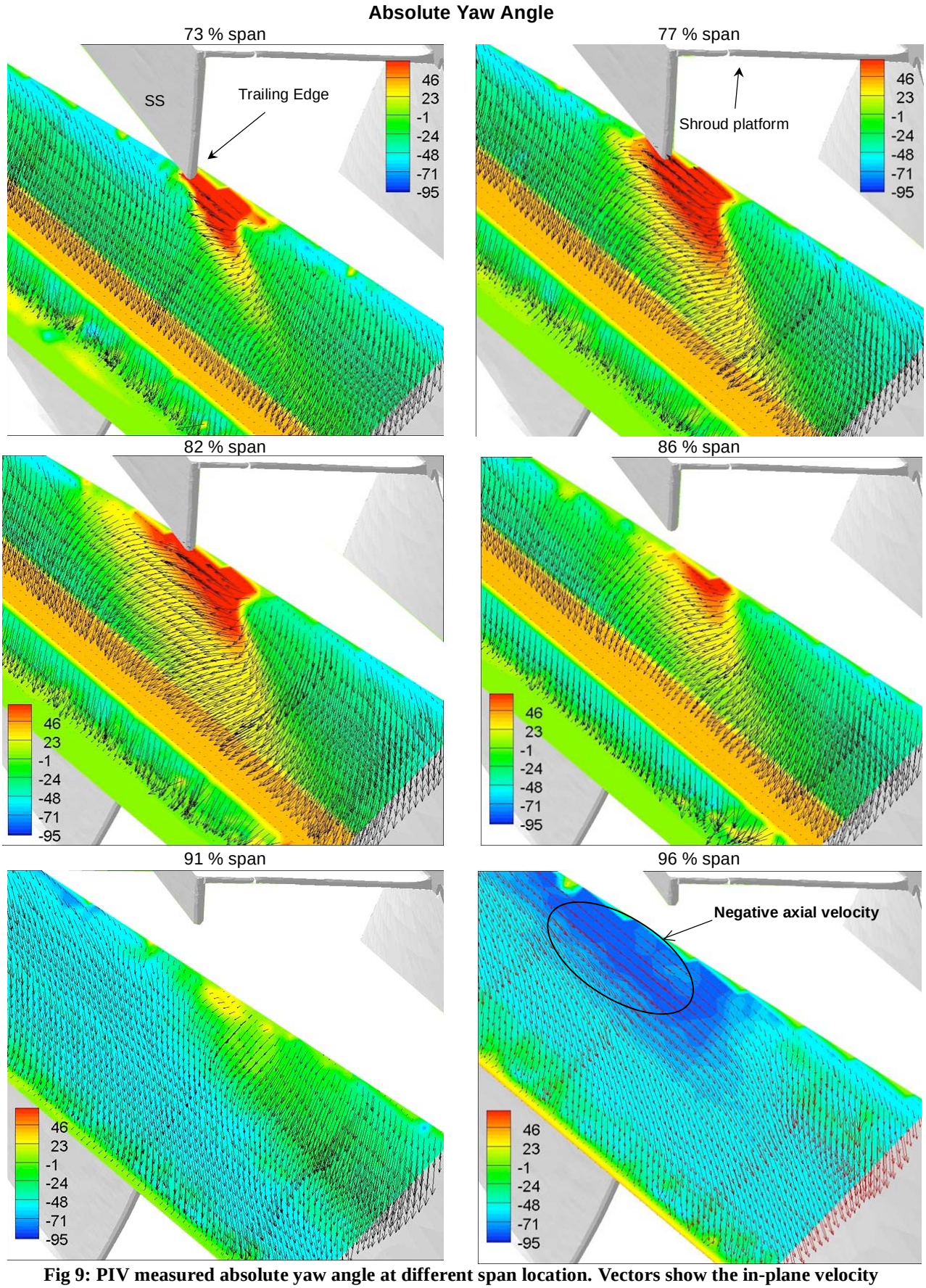

Fig 9: PIV measured absolute yaw angle at different span location. Vectors show the in-plane velocity component – Interstage region

This flow feature, although quite unusual in turbomachinery blades, has been already reported in low aspect ratio high turning NGV in previous investigation (Pullan et al. [25]). The sense or rotation from pressure side to suction side is consistent with those studies. This process is enhanced by high different blade loading at the same span between the blade pressure and suction side. Due to the partial covering of the shroud platform this different blade loading might be enhanced.

The combination of the passage vortex and the vorticity shed from the trailing edge pushes underturned and low momentum fluid towards the suction side. Moving farther downstream, the yaw angle gradient is decreasing showing mixing of the vortex structures. These vortical structures generate losses, known as secondary losses, as they dissipate and mix downstream of the blade row. A clear evidence of this process is the relative total pressure reduction measured by the FRAP probe in the axial plane located at 165% tip chord position (location shown in Figure 11).

Figure 12 shows the measured relative total pressure coefficient on this plane. The data are derived by retrieving the signal at one rotor blade position (blade passing fraction equal to T/T_0=1.85). The rotor trailing edge is shown in the pictures as well as the suction and pressure sides. The secondary flow field is computed at each time step using relative velocities and is defined as follows:

$$\vec{u}_{\text{sec}} = \vec{u}_i - \left(\vec{e}_{mean}\vec{u}_i\right)\vec{e}_{mean}$$

The velocity $\vec{u}_{\text{sec}}$ is the local secondary flow vector, $\vec{u}_i$ the local flow vector while $\vec{e}_{mean}$ is the mean unit vector circumferentially averaged and computed at each time step. A local pressure decrease is measured in the wake region and in an extended area corresponding to the cavity region and secondary flows areas. Two secondary counter rotating vortex structures are visible (A and B in Figure 10) and they push low momentum fluid coming from the wake towards the blade suction side. In this region a local relative total pressure reduction is measured. The vortex shed from the trailing edge is not visible anymore. By comparing the data from PIV and FRAP, the structure A is identified as a passage vortex while structure B is thought to be the vortex originated by the sudden flow expansion after the shroud cut back. The latter might have been enhanced by the pressure difference from PS and SS. This structure could not be seen in the PIV data because the laser sheet could only light up to 97% span but is visible in the FRAP plane located further downstream in axial direction. Figure 11 shows a meridional view of the interstage region with a schematic of these flow structures. Vortex B is created during the flow expansion downstream of the shroud cut back. Then, due to the contoured endwall, the vortex entrained into the main flow and is visible in the FRAP plane location.

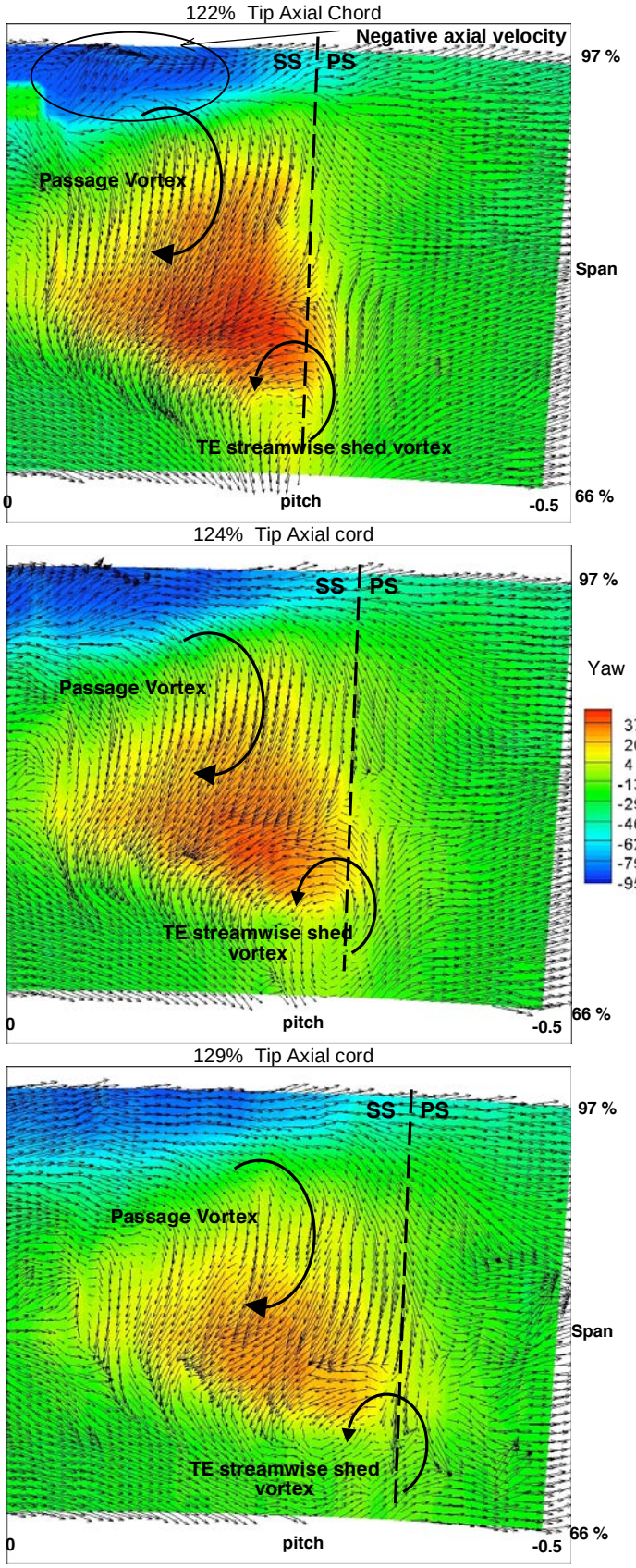

Fig 10: PIV Measured absolute yaw angle at different axial plane. Vectors show the in-plane velocity component – Interstage region

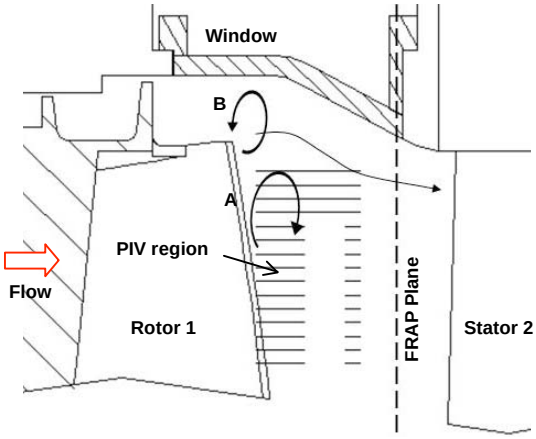

Fig. 11: Schematic of flow structures in the interstage region

Evidence of this structure can be seen from the measured data in the cavity downstream of the second rotor as described in Part II of this work. In Figure 12 the time evolution of the relative total pressure coefficient is plotted as a function of the measurement position with respect of the stator blade. In Figure 13a, a span location of 80% is selected where the secondary flows have the highest interaction. The vertical dashed line defines the approximate position of the second stator leading edge (slightly varying with the radial position) while the horizontal line defines the blade period time fraction shown in Figure 12. Relative total pressure reduction is associated with the vortical structure described previously and is observed with an inclined pattern showing that this feature is moving with the rotor blade. For a better visualization, the same scale is selected in Fig 12 and 13.

Differences between the passage vortex A and the tip leakage vortex B are not visible and only a broad total pressure drop is detected. However, a difference in the total pressure reduction is observed when the feature approaches the second stator leading edge. Region of low relative total pressure have different intensity when they move close to the stator leading edge. Due to the blockage effect of the stator leading edge, the vortical structure's diameter grows. The relative total pressure drop decreases at this point. According to Kelvin's theorem, the circulation around a streamtube remains constant; therefore, in incompressible flows, if the vortex diameter grows the secondary kinetic energy decreases. Thus dissipation by viscous effects is weakened and a local reduction of relative total pressure drop occurs corresponding with the stator leading edge (Figure 13a). A possible reason for this reduction might be attributed to a local reduction of loss generation in this location. Similar unsteady mechanism but at the hub section has been reported by Schlienger et al. [1].

In Figure 13b the time distance diagram is presented showing data measured at the blade midspan location. At this location, secondary flows are not present; the flow field is dominated by the rotor wake and the potential field of the second stator.

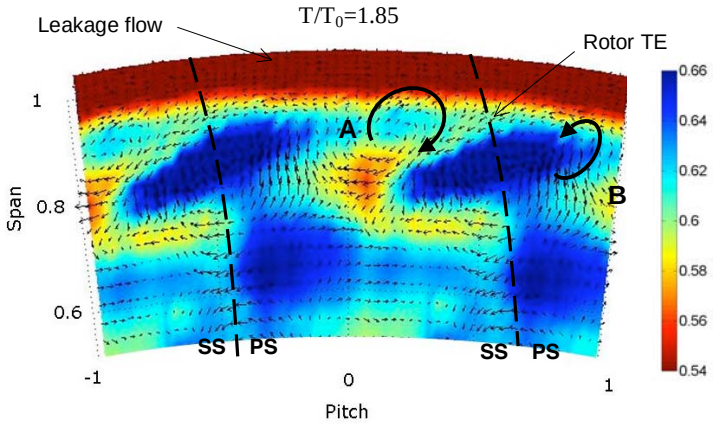

Fig. 12: Relative total pressure coefficient and secondary flow vectors – Interstage region – FRAP plane

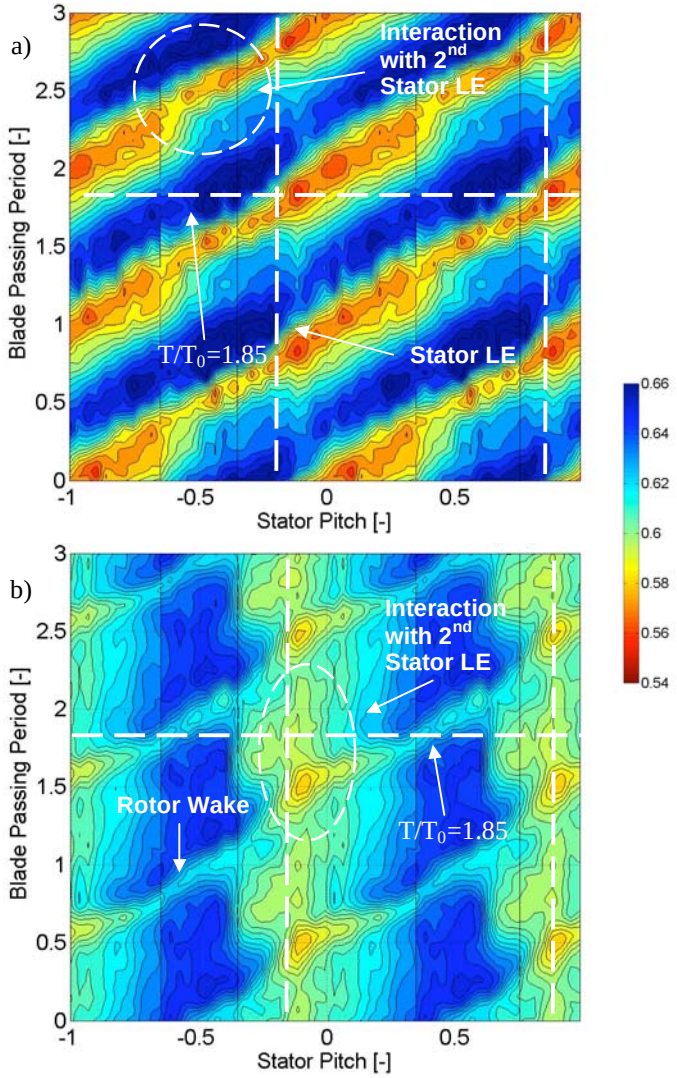

Fig. 13: Time distance plot of relative total pressure coefficient at a) 80% span and b) 50% span – FRAP Plane

The rotor wake is shed by the trailing edge and is transported downstream approaching first the suction and then the pressure side of the second stator blade. In the middle of the

stator passage (pitch around 0.4 in Figure 13b), the wake is transported downstream with very little disturbances.

However while the rotor blade is moving, the wake experiences a compression due to the stator blockage effect; then it flips around the leading edge and impinges on the pressure side. If the wake is considered as a vortical structure with two counter rotating vortex sheets, according to the Kelvin's theorem, the velocity difference is amplified when the wake is compressed. This results in an increased velocity gradient inside the wake that results in an increase in the mixing losses. This process is shown in Figure 13b around pitch equal to 0 where a broad area of increased relative total pressure drop is measured.

Vortex – wake interaction

Figure 14 shows the calculated radial vorticity at different blade height positions. An interpolation procedure has been applied to project the measured data into a plane with the same radii. Negative and positive radial vortices are shed by the blade trailing edge showing a vortex street behavior. The vorticity shed from the pressure side is stronger due to the much steeper velocity gradient in the thin boundary layer. Moving radially to the tip, an interaction between radial and streamwise vorticity occurs due to the presence of the passage vortex and the trailing edge vortex. Thus the radial vorticity component decreases on the suction side. It remains almost unchanged on the pressure side. Approaching the tip region, starting from 89% span, radial vorticity is no longer observed due to the presence of the shroud platform. The main flow, as discussed previously, experiences a sudden expansion due to the uncovered tip region of the suction side. This expansion is probably damping the radial vorticity on both pressure and suction sides while enhancing the circumferential vorticity evolution as measured in the cavity region.

Several experimental and numerical investigations have been focused on the trailing edge vortex street shedding in turbine cascades. However, measurements of shed vorticity in rotating machines are quite uncommon. Frequency shedding is a function of trailing edge thickness. Strouhal number is the ratio between the convective velocity of the eddies and the main velocity of the flow.

$$Sr = \frac{fD}{U}$$

where U is the circumferentially velocity magnitude at the exit of the blade in the relative frame of reference. Cicatelli and Sieverding [26] performed an investigation in turbine cascade blade with similar exit Mach and Reynolds number. The Strouhal number was derived by measured frequency on the blade trailing edge corresponding to 0.27. With the same Sr number, the frequency calculated in the present work is equal to 23.4 kHz. This frequency is about 13 times higher than the blade passing frequency (1.8 kHz) and is higher than values from simulations of turbine stages (Sondak and Dorney [27]). The knowledge of the shedding frequency can be important during the design phase to prevent blade resonances.

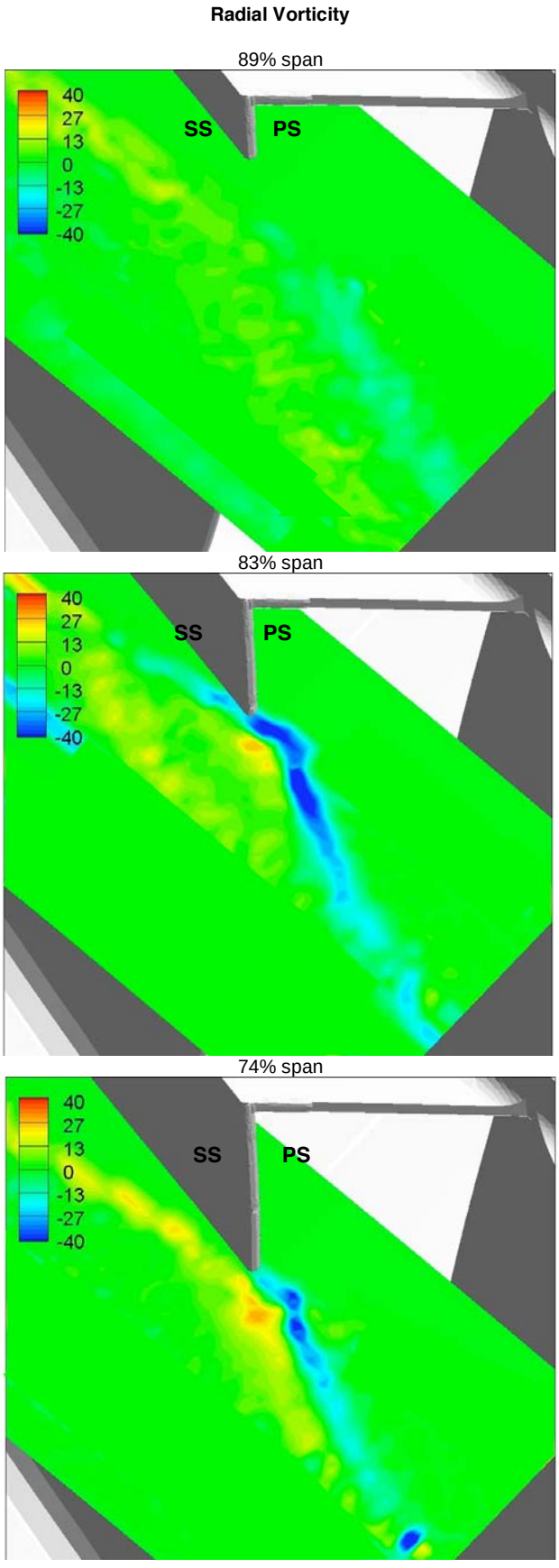

Fig 14: PIV measured radial vorticity at different blade span location.

DISCUSSION

A detailed analysis of the flow field in a partially shrouded turbine has been carried out. The focus is on the flow interaction on the main flow field in the interstage zone (Part I) and the kinematics in the cavity region (Part II).

The non-axisymmetric shroud geometry induces a highly three-dimensional flow field at the exit of the rotor. In both rotors similar flow features have been observed. The sudden change of area in the blade passage causes an expansion of the fluid of the main passage that interacts with the leakage flow. After the expansion, the fluid rolls up from the pressure to the suction side of the blade and interacts with the passage vortex.

The unsteady analysis of the pressure evolution shows that a large variation of relative total pressure up to 18% between vortex core and main flow is measured during the interaction with the second stator leading edge. This process is modulated by the blade passing frequency. Vortex kinematics analysis can explain the lower loss production measured in the area corresponding to the position of the second stator leading edge.

At midspan, the rotor wake has a lower variation in total pressure. In the middle of the wake a total pressure reduction of around 8.2% has been measured. A loss increase is measured when the wake impinges the stator leading edge due to compression and higher dissipation. Thus, the unsteady loss generation occurring at midspan is opposite to what is observed in the secondary flow region.

This analysis shows that the unsteady loss generation in this low aspect ratio geometry is more pronounced in the region of secondary flow interaction rather than at midspan. Therefore secondary flow aspects should receive more attention in the aerodynamic design.

Possible ways to increase aerodynamic performances can be found in the optimized design of the rotor blade tip and the subsequent NGV leading edge. To increase mixing in the tip region and reduce the unsteady vortex diffusion effect, the axial distance between rotor and stator could be increased at the tip by adopting a backward swept stator profile. Also the stator leading edge profile should take into account the higher angle fluctuations resulting in large incidence variation occurring in this area by increasing the leading edge radius.

CONCLUSION

A unique set of steady and unsteady data has been acquired by means of different measurement techniques (Stereo PIV and FRAP) in a partially shrouded multistage axial turbine. Owing to the combination of flow velocimetry and pressure measurements, the flow kinematics and loss generation mechanism have been verified.

Stereoscopic Particle Image Velocimetry has been compared with FRAP unsteady pressure measurements and 5HP at the exit of the turbine section, and they show a good agreement. In the interstage region the mean value of pneumatic averaged measurements and the time average PIV data shows higher differences moving radially through the blade tip. The high degree of unsteadiness in this region and the high pitch angle due to the proximity of the countered endwall might be at the origin of this behavior. However, the pneumatic data lay always inside the range of variation of the PIV data over one blade passing period.

The interaction of vortex structures has been studied in the interstage tip region. The passage vortex after the blade throat grows and, due to the uncovering of the blade throat, passes over the shroud platform. Together with the tip passage vortex, a vortex is formed due to a sudden flow expansion at the trailing edge of the shroud. These structures entrain low momentum fluid from the wake and generate a local loss core measured farther downstream by FRAP probe.

Analysis of the unsteady signals shows that this process is not continuous but triggered by the blade passing period. Unsteady loss generation occurs in location corresponding with the second stator leading edge. Vortex diffusion and wake compression has been observed from the measured relative total pressure.

The present study has provided a large database of unsteady data in a multistage turbine. Designers can profit from a better understanding of unsteady flow physics and achieve improvement in the aerodynamic blade/shroud design. For this purpose some design suggestions have been proposed to reduce the unsteady interaction between flow structures of the first rotor and leading edge of the following stator row.

AKNOWLEDGMENTS

The support of the Alstom-ETH research and development forum "Center of Energy Conversion" and the financial support of Alstom Power are acknowledged. The authors gratefully acknowledge Alstom Power Switzerland for their kind permission to publish the results presented in this paper. In particular, thanks are due to Dr Michael Loetzerich for his support and suggestions during the course of this research activity.

REFERENCES

[1] Schlienger J., KalfasA.I., Abhari R.S. "Vortex-Wake-Blade Interaction in a shrouded Axial Turbine" ASME Journal of Turbomachinery Oct 2005, Vol 127.

[2] Miller R.J., Moss R.W., Ainsworth R.W., Horwood C.K., "Time-Resolved Vane-Rotor Interaction in a High-Pressure Turbine Stage" ASME J. Turbomach. 125, 1 (2003)

[3] Wernet M.P., "Application of DPIV to study both steady state and transient turbomachinery flows" Optics & Laser Technology 32 (2000) 497-525.

[4] Balzani N., Scarano F., Riethmuller M.L., Breugelmans F.A.E., "Experimental Investigation of the Blade-to-Blade in a Compressor Rotor by Digital Particle Image Velocimetry" ASME J. Turbomach. 122, 743 (2000)

[5] Sanders A.J., Papalia J., Fleeter S., "Multi-Blade Row Interactions in a Transonic Axial Compressor: Part I – Stator Particle Image Velocimetry (PIV) Investigation" ASME J. Turbomach. 124, 2002

[6] Uzol O., Chow Y.C., Katz J., Meneveau C., "Experimental Investigation of Unsteady Flow Field Within a Two-Stage Axial Turbomachine Using Particle Image Velocimetry" ASME J. Turbomach. 124, 2002

[7] Liu B., Wang H., Liu H., Yu H., Jiang H., Chen M., "Experimental Investigation of Unsteady Field in the Tip Region of an Axial Compressor Rotor Passage at Near Stall

Condition with Stereoscopic Particle Image Velocimetry" ASME J. Turbomach. 126, 360 (2004)
[8] Göttlich E., Woisetschläger J., Pieringer P., Hampel B., Heitmeir F., "Investigation of Vortex Shedding and Wake-Wake Interaction in a Transonic Turbine Stage using Laser-Doppler-Velocimetry and Particle Image Velocimetry" ASME paper GT2005-68579.
[9] Porreca L., Behr T., Schlienger J., Kalfas A.I., Abhari R.S., Ehrhard J., Janke E., "Fluid Dynamics and Performance of Partially and Fully Shrouded Axial Turbines" ASME Journal of Turbomachinery Oct 2005, Vol 127.
[10] Prasad, A.K., 2000, Stereoscopic Particle Image Velocimetry, Exp. Fluids, 29, 103-116.
[11] Kähler, C.J., Sammler, B., Kompenhans, J., 2002, Generation and Control of Tracer Particles for Optical Flow Investigations in Air, Exp. Fluids, 33, 736-742.
[12] Mellin A., "Tracer Particles and Seeding for Particle Image Velocimetry", Meas. Sci. Technology 8 (1997) 1496-1416.
[13] Zang, W.J., Prasad, A.K., 1997, "Performance Evaluation of a Scheimpflug Stereocamera for Particle Image Velocimetry", Applied Optics, 36, 8738-8744.
[14] Soloff, S.M., Adrian, R.J., Liu, Z-.C., 1997, "Distortion Compensation for Generalized Stereoscopic Particle Image Velocimetry", Meas. Sci. Technol. 8, 1441-1454.
[15] Westerweel, J., Dabiri, D., Gharib, M., 1997, "The Effect of a Discrete Window Offset on the Accuracy of Cross-Correlation Analysis of Digital PIV Recordings", Exp. Fluids, 23, 20-28
[16] Scarano, F., Riethmuller, M.L., 1999, "Iterative Multigrid Approach in PIV Image Processing with Discrete Window Offset", Exp. Fluids, 26, 513-523.
[17] Westerweel, J., 1994, "Efficient Detection of Spurious Vectors in Particle Image Velocimetry", Exp. Fluids, 16, 237-247.
[18] Raffel M., Willert C. and Kompenhans J. "Particle Image Velocimetry – A Practical Guide" 1998 Berlin Springer
[19] Willert, C.E., Gharib, M., "Digital particle image velocimetry", Experiments in Fluids, 10 pp. 181-193
[20] Keane, R.D., Adrian, R.J., "Theory of cross correlation analysis of PIV images" Applied Scientific Research 1992, pp.191-215
[21] Lawson N.J., Wu J. "Three-dimensional Particle Image Velocimetry: Error Analysis of Stereoscopic Techniques" Measurement and Science Technology Vol. 8 894-900, 1997
[22] Porreca L., Hollenstein M., Kalfas A.I., Abhari R.S., "Turbulence Measurements and Analysis in a Multistage Axial Turbine", ISABE 4-9 September 2005, Munich.
[23] Treiber M., Kupferschmied, P. and Gyarmathy, G., 1998 "Analysis of the Error Propagation Arising From the Measurements with a Miniature Pneumatic 5-Hole Probe" XIVth Symposium on Measuring Techniques for Transonic and Supersonic Flows in Cascade and Turbomachines.
[24] Wallis A.M., Denton J.D., Demargne A.A.J., "The Control of Shrouded Leakage Flows to Reduce Aerodynamic Losses in a Low Aspect Ratio, Shrouded Axial Flow Turbine" Journal of Turbomachinery, April 2001, Vol 123.
[25] Yun Y.I., Porreca L., Kalfas A.I., Song S.J., Abhari R.S., "Investigation of 3D Unsteady Flows in a Two Stages Shrouded Axial Turbine Using Streoscopic PIV and FRAP – Part II: Kinematics of Shroud Cavity Flow" ASME Paper GT2006-91020, Barcelona 2006
[25] Pullan G., Denton J., Dunkley M., "An Experimental and Computational Study of a Streamwise Shed Vortex in a Turbine Stage". ASME Journal of Turbomachinery, April 2003, vol 125.
[26] Cicatelli G., Sieverding C.H., "The Effect of Vortex Shedding on the Unsteady Pressure Distribution Around the Trailing Edge of a Turbine Blade" ASME Journal of Turbomachinery, October 1997, Vol 119.
[28] Sondak, D.L. and Dorney D.J., "Simulation of Vortex Shedding in a Turbine Stage" ASME Journal of Turbomachinery, 121pp. 428-435.